Field emission microscopy pattern of a single-crystal diamond needle under ultrafast laser illumination

M. H. Mammez, M. Borz, Ivan Blum, Simona Moldovan, L. Arnoldi, S. Idlahcen, A. Hideur, V. I. Kleshch, A. N. Obraztsov, Angela Vella

IOP Publishing New J. Phys. 21 (2019) 113060 https://doi.org/10.1088/1367-2630/ab5857

New Journal of Physics
The open access journal at the forefront of physics

Deutsche Physikalische Gesellschaft DPG
IOP Institute of Physics

Published in partnership with: Deutsche Physikalische Gesellschaft and the Institute of Physics

OPEN ACCESS

RECEIVED
2 July 2019

REVISED
5 November 2019

ACCEPTED FOR PUBLICATION
12 November 2019

PUBLISHED
29 November 2019

PAPER

Field emission microscopy pattern of a single-crystal diamond needle under ultrafast laser illumination

M H Mammez[1], M Borz[1], I Blum[1], S Moldovan[1], L Arnoldi[1], S Idlahcen[2], A Hideur[2], V I Kleshch[3], A N Obraztsov[3,4] and A Vella[1]

[1] Groupe de Physique des Matériaux UMR CNRS 6634, Normandie Université, Université-INSA de Rouen, Avenue de l'Université BP 12,F-76801 Saint Etienne du Rouvray, France

[2] CORIA UMR CNRS 6614, Normandie Université, Université-INSA de Rouen, Avenue de l'Université BP 12, F-76801 Saint Etienne du Rouvray, France

[3] M. V. Lomonosov Moscow State University, Department of Physics, Moscow 119991, Russia

[4] University of Eastern Finland, Department of Physics and Mathematics, Joensuu, FI-80101, Finland

E-mail: angela.vella@univ-rouen.fr

Keywords: nanoemitters, field emission, ultrafast laser, electron spectroscopy, diamond

Abstract

We report herein on the spatial beam properties of a field emission electron source based on a single-crystal diamond needle illuminated by ultrashort light pulses. We show that the increasing of the laser intensity strongly modifies the emission pattern, leading to the emergence of a new emission region at high peak power. This region is situated on the opposite side of the diamond needle to the one irradiated by the laser. By spatially-resolved energy spectrometry, we prove that the electrons emitted from this region are governed by a multi-photon absorption process. The occurrence of this emission pattern can be explained by accounting for the inhomogeneous distribution of the optical field enhancement and the laser absorption induced by light diffraction within the nanometric needle. The numerical simulations performed on a real sub-wavelength tip confirm this localization of the optical field enhancement and reveal that the electrons trajectories match the spatial beam distribution evidenced experimentally. This work underlines the need to closely monitor the surface roughness of the field emitter as well as the laser illumination conditions to finely control its emission pattern.

Introduction

During the past decades, the ultrashort electron pulses have attracted significant interest for a wide range of applications particularly in the field of electron microscopy [1–4] and portable x-ray sources [5, 6]. For instance, the metallic field-emitters (in particular tungsten tips) triggered by ultrashort (femtosecond) laser pulses have already been integrated into electron guns of ultrafast electron microscopes for a decade now [7, 8]. In addition, the carbon-based materials (such as carbon nanotubes (CNT), carbon or diamond nano-cones, diamond nano-crystals, etc) have been intensively studied as cold cathodes [9–11]. Recent works report on their high stability and brightness under laser illumination [12–15]. In particular, the diamond received a lot of attention due to its unique properties: chemical inertness, mechanical stability and high thermal conductivity [16, 17]. In this sense, recent studies have demonstrated that diamond is an excellent candidate for field-emission cathode, in the dark or under ultrafast laser illumination [12, 18–21].

The electron emitters constituted by single-crystal diamond needles, or nano-diamond-coated tips have demonstrated excellent mechanical stability and robustness under laser illumination and strong electric current. Under femtosecond (fs) laser illumination, the electrons can be photo-excited because multi-photon excitation becomes efficient. In the case of single-crystal nano-needles, the photo-excitation remains the dominant cause of electron emission at both low and high repetition rate of the laser, due to the high thermal conductivity of the diamond [20, 21].

We report in this paper, for the first time, on the changes of the emission patterns from a single-crystal diamond needle upon sub-ps laser illumination. The main point highlighted by direct observations is the occurrence of a large additional emission region along the border of the detector on one side of the electron emission microscopy (EEM) pattern.The spatially-resolved energy spectrometry proved that the emission process within this area is principally driven by a photoassisted emission resulting from multi-photon absorption. We tentatively explain the origin of this phenomenon by self-focusing of the electrons emitted from the shank of the nano-needle by surface asperities by using the simulated optical field distribution and the optical absorption map in three dimensions. The simulations identify the presence of areas of strong absorption and field enhancement at the surface of the nano-needle, located on the opposite side of the laser illumination. By transmission electron microscopy (TEM), we have imaged the surface asperities further schematized in an effort to numerically compute the trajectories of electrons emitted from the shank of the nano-needle. The paper is organized in three sections. In the first section, the sample preparation procedure and the experimental set-up are presented. The second section is devoted to the presentation of the experimental results for emission in dark and under laser illumination. In the third section, the experimental results are discussed and the numerical simulation are presented. Eventually, the conclusions are drawn.

Experimental setup

Samples

The diamond needles were prepared by chemical vapor deposition (CVD) growth of a polycrystalline film on a silicon substrate using a hydrogen-methane gas mixture activated by a direct current discharge. After growth, the films were etched by selective oxidation in air at about 900 K for several hours until complete gasification of disordered carbon material from the CVD film. After oxidation, micrometer scale diamond crystallites of needle-like pyramidal shape with the height coinciding with the á100ñ direction remain on the silicon substrate. The apex radius of the diamond needle is of some tens of nanometers. Detailed description of the fabrication processes, shape and structural parameters of the diamond needles can be found elsewhere [22, 23]. Individual diamond needles were fixed on a tungsten support tip either by conductive glue using a micromanipulator under an optical microscope or using ion beam induced deposition of platinum in a focused ion beam apparatus [20]. Typical TEM images obtained for one of the samples analyzed in this work are displayed in figure 1. The dimensions of this sample are: length $=$ 21(1) μm, and local apex radius R $=$ 50(5) nm.

Electron emission measurement

The diamond sample was used as an electron source for field emission (FE) measurements. It was placed in an ultra-high vacuum chamber at pressure of 4×10^{-10} mbar. A bias voltage $-V_{tip}$ was applied to the tungsten support tip. The electron kinetic energy spectrum was measured thanks to a set of retarding concentric hemispherical grids with an entrance at about 3 cm from the tip apex (the grids were polarized as shown in the sketch of the experimental apparatus in figure 2). The kinetic energy of the emitted electrons can be measured with a resolution of 0.5% of eV_{tip} , where e is the elementary (positive) charge. The detector was composed of two micro-channel plates mounted in chevron configuration and coupled with a phosphorescent screen. Impacts on the phosphorescent screen were recorded by using a fast CCD camera in order to obtain 2D emission maps. Each detected impact corresponds to one electron. The number of impacts per image corresponds to the current detected and was determined *a posteriori*. More details on the set-up and current measurements are available in [20].

Laser illumination

The sample was illuminated by an ultrafast ytterbium-doped fiber-based laser operating at 1040 nm. The laser system consists in a fiber-based chirped-pulse amplifier delivering short pulses with few microjoules of energy at repetition rates varying from 0.9 to 18 MHz. To reach even lower repetition rates, a free-space acousto-optical modulator (AOM) was placed at the laser output. In the following analyses the repetition rate was fixed to 40 kHz due to the limitation of our detection system. The pulse duration of 700 fs was measured by an autocorrelator at the laser output just after the AOM. More details on our home-made laser operation are reported elsewhere [20]. The laser beam has been focused on the diamond nano-needle through a set of mirrors and lenses, as shown in figure 2. The beam size measured before the lens is of about 10 mm and the beam waist at the focal point is 45 μm (diameter at $1/e^2$ level). This means that the whole needle is illuminated by the laser beam.

All measurements were performed at room temperature.

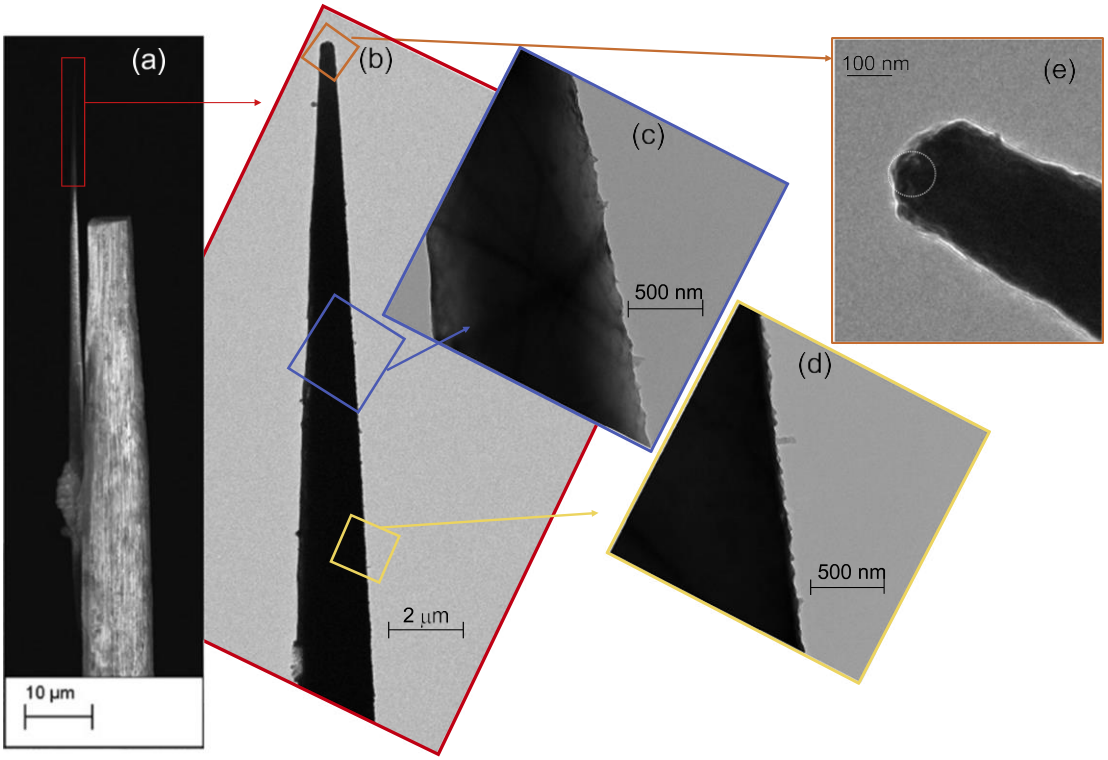

Figure 1. TEM images of the single-crystal diamond needle fixed on a tungsten tip.

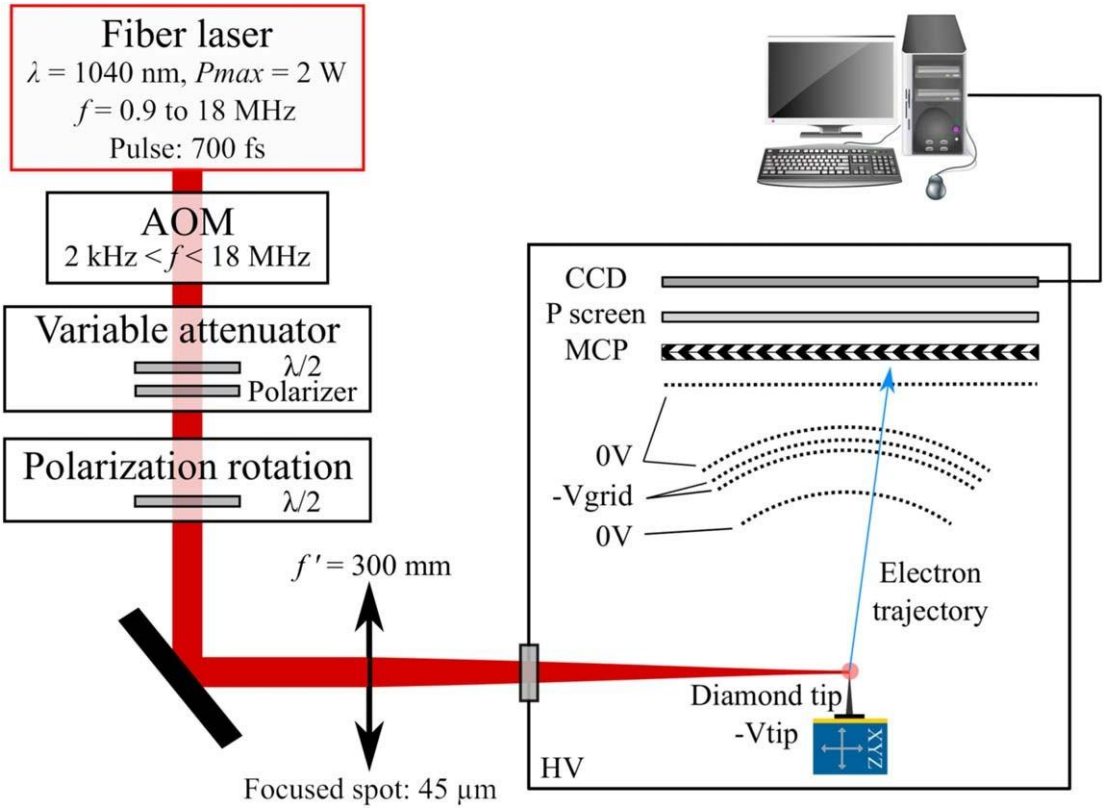

Figure 2. Experimental setup—AOM: acousto-optical modulator; MCP: micro-channel plates. $V_{MCP,in}$ = 290 V; $V_{MCP,out}$ = 1700 V; $V_{P\ screen}$ = 2790 V.

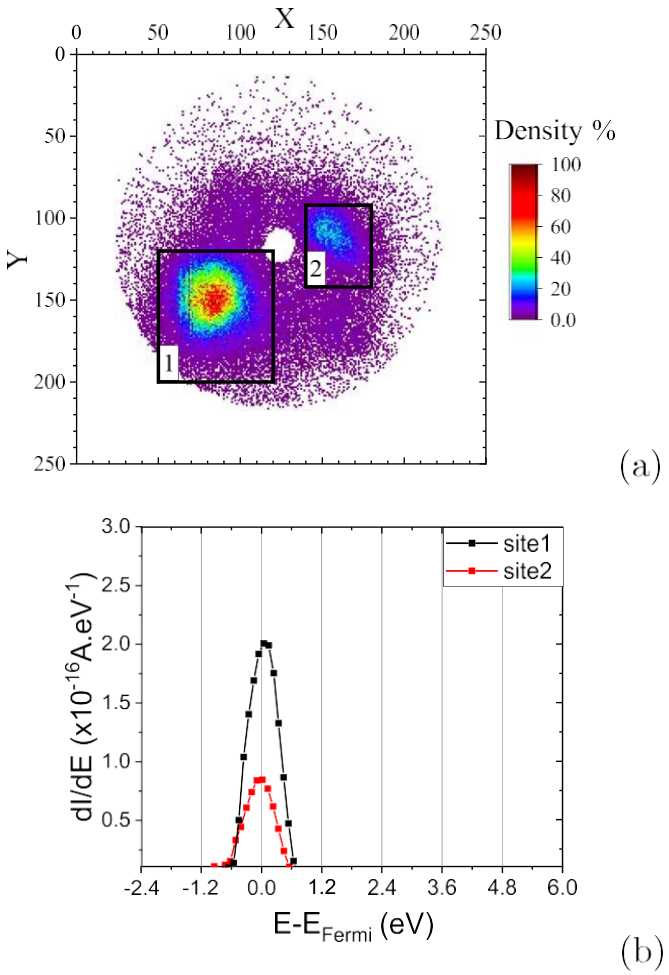

Figure 3. (a) EEM pattern in the dark. The (*X*, *Y*) coordinates indicate the position on the CCD camera in number of pixels. The color map corresponds to the normalized density of impacts. (b) Electron energy spectra at $V_{tip} = 300$ V of the sites 1 (black dots) and 2 (red dots) defined in (a).

Experimental results

The field electron emission in dark (without laser illumination) from similar diamond needles as the ones investigated in this work was reported in previous papers by Kleshch *et al* [19], Borz *et al* [20] and Terresin *et al* [24]. Two different behaviors in Fowler–Nordheim (FN) coordinates were reported: a linear behavior [18, 20], as for the case of metallic field emitters, or a saturated behavior, as for the semi-conducting field emitters [19, 24]. Even if non-doped bulk diamond is a wide-bandgap semiconductor, the metallic behavior was explained by transport of electrons via numerous defects and impurities at the surface of the diamond needle. In the present work, the metallic behavior was observed after preliminary 'cycling' of the sample, consisting in the successive increasing and decreasing of the applied voltage between 200 and 1000 V for several cycles. During the cycling occasional irregularities such as adsorbed molecules structural defects etc are removed from the surface due to the high intensity current resulting from field and ion emission.

Thereafter, the emission pattern and the spatially-resolved energy spectra were measured in dark and under laser illumination, at $V_{tip} = 300$ V.

The electron emission pattern was recorded by the 256 × 256 px CCD camera. The pattern recorded in dark is depicted in figure 3(a). It identifies that impacts are concentrated in two areas, the projections on the detector of the emissive areas of the diamond field emitter. These areas could correspond to two asperities of the disordered pure (amorphous) carbon located on the apex of the diamond needle [22]. Similar patterns consisting of few emission spots were observed in previous studies of diamond field emitters [19].

On our 2D detector, the emitted current can be integrated in a restrained zone in order to extract the spectrum of each emission site. The two selected areas on the detector system are indicated by two rectangles in figure 3(a). The energy spectra were calculated by the derivation of the electron current measured with a scan resolution of 0.1 V over 100 ms. After the use of Savitzky–Golay smoothing filter over 20 adjacent points on the measured current, the spectra are calculated. The two emission sites show a single peak, as reported in

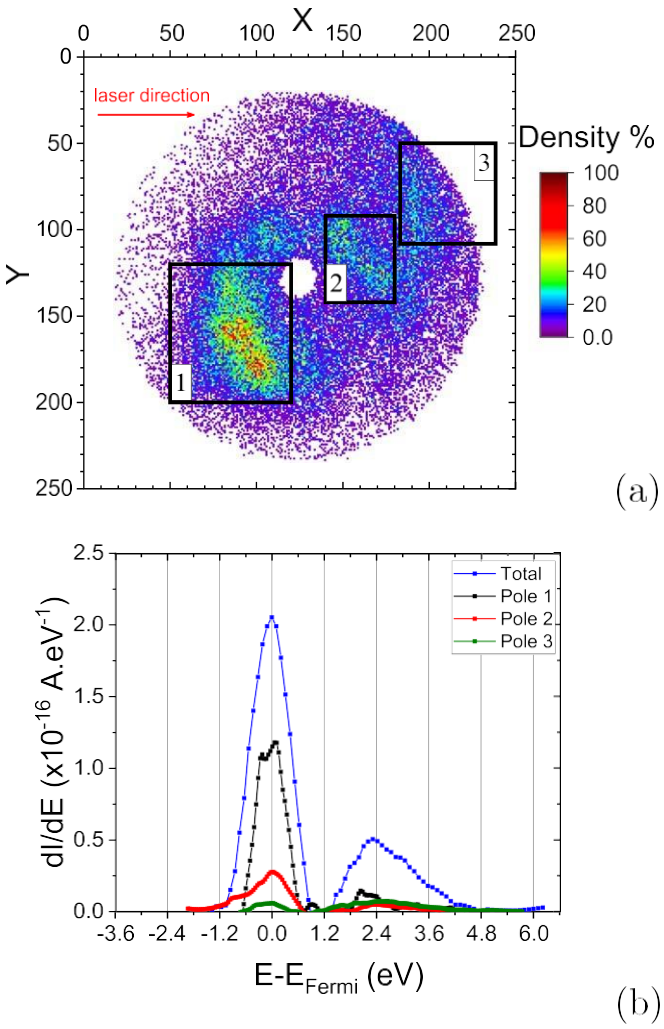

Figure 4. (a) EEM pattern and (b) energy spectra of the sites 1 (black dots),2 (red dots) and 3 (green dots) defined in (b), at V_{tip} = 300 V under laser illumination with a 40 kHz repetition rate I_{peak} = 13 GW cm^{-2}. The (*X*, *Y*) coordinates indicate the position on the CCD camera in number of pixels. The colors map corresponds to the normalized density of impacts.

figure 3(b). Since the sizes of the two areas are different, only the shapes of the spectra are comparables, but not their amplitudes. Note that the current−voltage characteristics in linear and in FN coordinates are reported in [20], where the voltage emission threshold of 280 V and an emission current of 180 counts s^{-1} at 300V was measured.

When the sample is illuminated by the laser beam at I_{peak} = 13 GW cm^{-2}, the electron emission pattern changes, as depicted in figure 4(a). The changes in the emission current in linear and in the FN plots are reported in [20].The shape of the two sites changes from rounded to elongated. Moreover, a new emission area arises on the right-top side of the detector as indicated in figure 4(a) within the zone 3. The impacts collected on this side of the detector correspond to the electrons emitted at the opposite side of the laser illumination on the needle.

The spectra corresponding to the areas delimited in figure 4(a), are shown in figure 4(b) and are compared to the average spectrum integrated over the entire surface of the detector. This last (the average spectrum integrated on the entire surface of the detector) was already discussed by authors considering the photoassisted FE in [20], because photoassisted FE is observed when analyses were performed under laser illumination at a high applied voltages (300 V), however multi-photon emission happens at low applied voltages (<100 V). Here we discuss in details the differences between the spectra of the different regions in the emission pattern.

Two peaks are apparent, the first at the Fermi energy, as previously reported for emission in dark (or static emission) and the second peak at $E = E_F + 2.2$ eV, which corresponds to photoassisted field-emission, by the absorption of 1, 2 or 3 photons with energy of 1.2 eV. Note that all the three processes happen in the same time and contribute to the electron emission. This peak is wider because of the convolution of the different emission peaks related to these three photon absorption processes [20]. For sites 1 and 2, the static emission is stronger than the photoassisted field-emission. However, for site 3, the two emission processes have the same amplitude.

However the emission at the Fermi energy is probably due to residual emission from area 2. Therefore, on region 3, the laser contribution seems to be the only contribution, as confirmed at higher laser intensity.

To check if the change in the shape of sites 1 and 2 is due to additional emission spots, we divided these regions in three sub-regions and we calculated the spectrum corresponding to each of them. We obtained the same spectrum for all, which indicates that the emission is generated from the same region which expands under laser illumination. In fact, if a new region starts to emit under laser illumination, the peak at 0 eV in the spectrum should be negligible compared to the second peak at 2.4 eV, as reported for the region 3.

At higher laser intensity, $I_{peak} = 25$ GW cm^{-2}, the electron emission pattern continues to evolve, as reported in figure 5(a). The sites 1 and 2 remain visible while their relative intensity has strongly decreased. The emission region 3 is now larger and the emitted current is higher.

The spectra corresponding to these three areas are shown in figures 5(b), (c) and are compared to the overall spectrum integrated over the detector entire surface area. For the sites 1 and 2, two peaks are visibles similarly to the case of lower laser intensity. The first peak at the Fermi energy is followed by the second peak at the energy $E = E_F + 3$ eV, corresponding to the photoassisted field-emission. By increasing the laser intensity from 13 to 25 GW cm^{-2}, the second peak shifts toward higher energies and its amplitude increases. This indicates that the photoassisted FE becomes predominant and the number of photons involved in the process increases [20]. Moreover, at $I_{peak} = 25$ GW cm^{-2}, the static emission is still stronger than the photoassisted field-emission for sites 1 and 2.

In region 3, the peak at Fermi level was not identified. The variation of the current in region 3 is indicated on the right axis of the figure 5(c). For $E < E_F + 1.2$ eV, the current fluctuates and the spectrum can be calculated only for energy higher than 1.3 eV. Accordingly, the laser contribution appears to completely mask the static FE in region 3.

When V_{tip} is diminished below the static emission threshold and the sample is still illuminated, the emission is a purely photo-FE, being governed by multi-photon absorption [20]. In these conditions, only emission region 3 is visible on the detector. The spectra obtained for this case at different values of laser intensities ranging from 1.1×10^{10} W cm^{-2} to 1.8×10^{10} W cm^{-2} at 100 kHz repetition rate have been reported in [20].

Discussion

Under laser illumination, two different emission behaviors have been observed, depending on the laser intensity. At low intensity, the laser beam enhances the emission from the areas where the emission takes place in dark. Moreover, the energy spectra show that there is a contribution of photofield emission. At high intensity, the laser beam generates to a new emission region as compared to operation in dark. This area, referred as region 3 in the previous section, is on the right side of the detector, corresponding therefore to an emission area which is located in the opposite side to the facet of the diamond needle illuminated by the laser beam. Moreover, region 3 is large and cover almost entirely the right part of the detector. A similar behavior has been already reported for a carbon nanotube field-electron emitter [25]. It was shown that the pattern of the static emission can switch from a single point to a ring due to thermal-FE from the lateral surface of the nanotube caused by the temperature increase. In the present work, emission is observed only on one side of the detector, and the corresponding energy spectrum shows that the emission is purely photofield emission. In order to explain this asymmetric emission, the laser-tip interaction was computed using the finite-difference time domain method with a commercial software from Lumerical [26]. In this model, the tip is represented as a cone terminated by a hemispheric cap. This is placed in the simulation space using absorbing boundary conditions, in order to avoid the field reflections. For the wavelengths of 1040 nm, the material properties are taken into account by using the refractive index $n = 2.4 + i0.0032$. It is worth mentioning that we use here average values of refractive index and extinction coefficient typical for CVD diamond [27]. The beam is considered as a planar wave. The electric field and the divergence of the Poynting vector (which correspond to the absorbed energy) are calculated in all the simulated space, for a completed optical cycle. The results obtained on the small volume of $350 \times 350 \times 350$ nm^3 close to the apex, are reported in figure 6.

The electric field and the absorption map are perfectly symmetric with respect to the axis of the needle. Therefore, if the laser-induced emission area is located at the apex of the sample, these results can not explain why the emitted electrons impact only the right side of the detector system. On the contrary, the numerical results obtained on a larger volume show an inhomogeneous distribution of the electric field and the absorbed energy (see figure 7). On the absorption cross section of figure 7(b), a few regions of higher absorption are visible on the shadowed side. These regions also correspond to the areas where the electric field is higher (figure 7(a)). The inhomogeneous enhancement of the electric field and the presence of high absorption areas have already been reported on metallic and non-metallic field-emitters and they have been associated to the diffraction of the light by the nanometric needle [28, 29]. The higher enhancement of the electric field at the opposite side of the

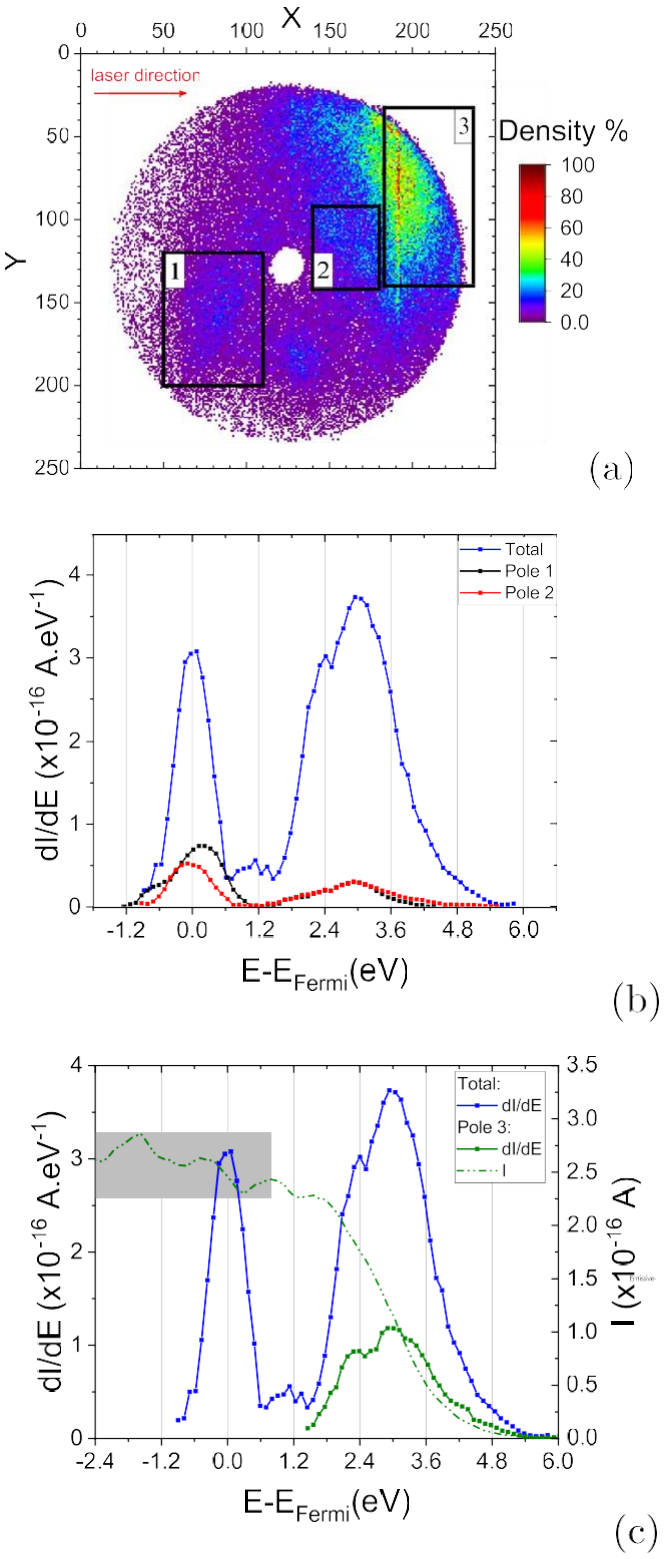

Figure 5. (a) EEM pattern, (b) energy spectra of the sites 1 (black dots) and 2 (red dots) and (c) energy spectra and emitted current from region 3 defined in (4 (a)), at V_{tip} = 300 V under laser illumination with a 40 kHz repetition rate I_{peak} = 25 GW cm^{-2}. The (*X*, *Y*) coordinates indicate the position on the CCD camera in number of pixels. The colors map corresponds to the normalized density of impacts. Gray area shows to the amplitude of the current fluctuations.

laser illumination is related to the high transparency of the needle and the excitation of the resonant surface modes first on the second interface and then on the first one. The areas of high absorption correspond to the zones of high temperatures and enhanced electric field within the specimen. Therefore, these are good candidates as electron emission sources but, in the case of emission from a flat surface on the shank of the needle, the electrons could not impact the detector, because of the limited field of view of the energy analyzer. However,

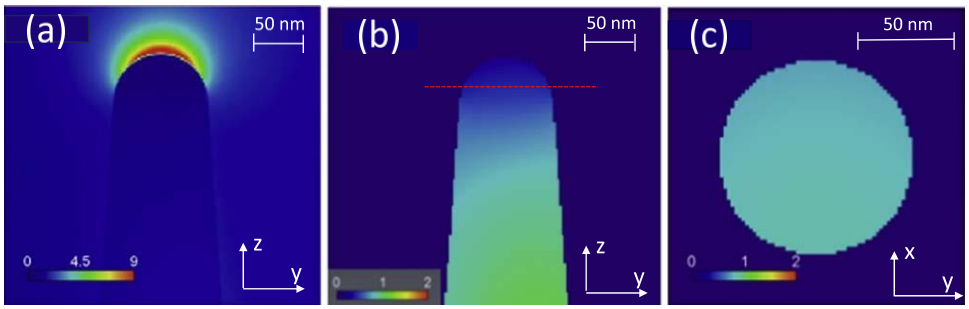

Figure 6. (a) (y, z) Cross section of the electric field distribution for an incident field of amplitude 1 V m^{-1}, corresponding to an intensity of 10^{-5} W cm^{-2}. The color scale is in V m^{-1}. (b) (y, z) and (c) (x, y) cross section of the absorbed energy for an incident field of amplitude 1 V m^{-1}. The color scale is in W m^{-3}. The red dashed line indicates the plane of the (x, y) cross section. The propagation direction of the laser is along the y axis and it is coming from the left. The laser is linearly polarized along the z axis.

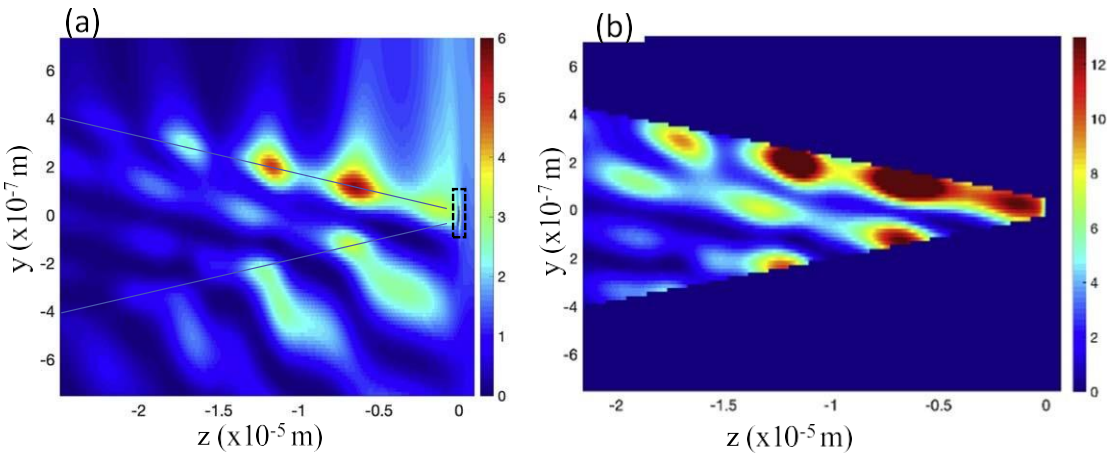

Figure 7. (a) (y, z) Cross section of the electric field distribution for an incident field of amplitude 1 V m^{-1}, corresponding to an intensity of 10^{-5} W cm^{-2}. The color scale is in V m^{-1}. The dashed box in black corresponds to the volume simulated in figure 6. (b) (y, z) cross section of the absorbed energy for an incident field of amplitude 1 V m^{-1}. The color scale is in W m^{-3}. The laser is propagating along the y axis from the bottom to the top. The laser is linearly polarized along the z axis.

diamond needles are not flat and many asperities are visible at the surface, as shown in figure 1 and such asperities can emit electrons due to additional electric field enhancement. Indeed, for asperities located in the areas of high field enhancement, the local field enhancement could be higher than at the needle apex, because the end radius of these asperities is of about 10 nm.

The trajectory of the electrons emitted by asperities on the larger area on the shank where the absorption is higher have been calculated numerically using the software Lorenz2D, taking into account the symmetry of revolution along the long nano-needle axis. As shown in figures 8(a), (b), three asperities of about 150 nm in height have been placed at 6, 12 and 18 μm away from the needle apex, corresponding to the maximum absorption and field-enhancement areas. These asperities are considered as electron emitters, together with the apex of the samples. The trajectories from the asperity close to the W support (tip) overlap the other trajectories (see figure 8(b)) and reach the detector system on the upper border (see figure 8(c)). The folding of the trajectories is influenced by the presence of the tungsten support (tip). As shown in figure 1(a), the diamond tip is fixed on a tungsten tip which terminates with a flat surface of about 10 μm in thickness. This charged surface is at the origin of the trajectories folding. The support structure strongly influences the trajectories of the electrons emitted by the asperities. A thicker tungsten support can induce a folding of trajectories from asperities far from the diamond/tungsten junction while a thinner tungsten support can avoid this folding phenomena.

In the case of the sample presented in figure 1, only the electrons emitted from the asperities close to the diamond/tungsten junction will be detected on the border of the detector system. The static electric field in this area is 50 times lower than the field at the apex of the sample. However, the enhancement of the optical field on the asperities can compensate this lack in static electric field.

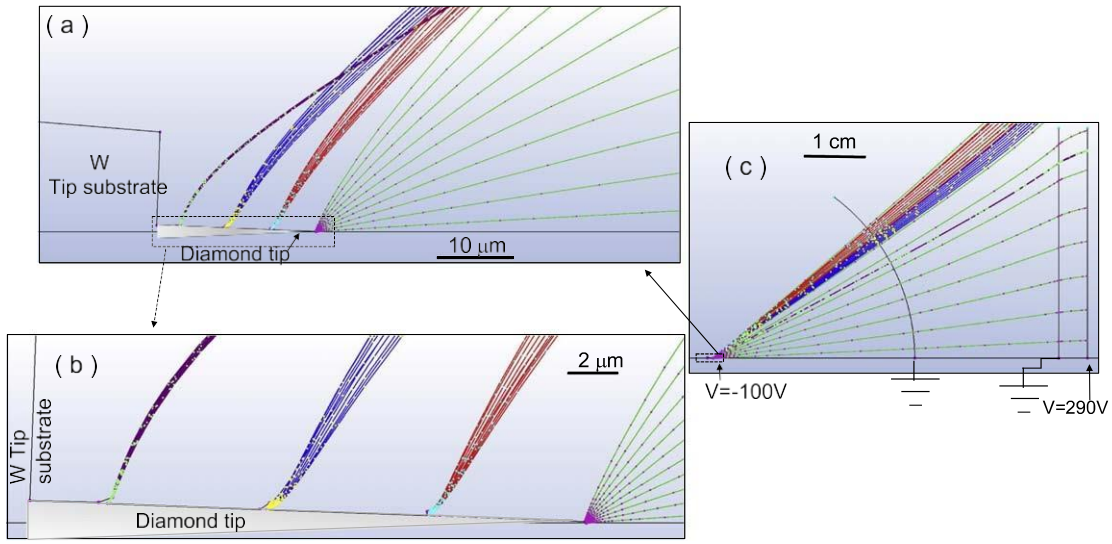

Figure 8. Simulation of the electrons trajectories from the diamond needle to the anode screen on different spatial scales: (a) 10 μm; (b) 1 μm and (c) 1 cm. The trajectories of the electrons emitted from the apex are represented in green, from the first, second and third asperity from the apex in red, blue and violet, respectively. The electrostatic configuration of the experimental analysis chamber is reported in figure (c).

Conclusion

The EEM pattern of a diamond single-crystalline field-emitter has been studied in dark and under sub-ps laser illumination. At low laser intensity, the EEM pattern shows little changes when compared to the pattern observed in dark. However, thanks to the spatially-resolved energy spectroscopy, the increase in the emitted current was associated to the photoassisted emission by multi-photon absorption which adds to the static emission. At high laser intensity, an additional emission region appears along the border of the detector corresponding to the shadowed side of the sample. This region of the pattern was attributed to the emission from asperities which are visible along the shank of the diamond needle.

Numerical simulations of optical field enhancement have shown a stronger enhancement on the shadowed side of the sample as against the illuminated one. Moreover, numerical simulations of electron trajectories from surface asperities have shown that the folding of trajectories strongly depends on the geometry (in particular the thickness) of the tungsten tip.

Two factors appear to affect the detection of electrons emitted from the asperities along the tip shank: the optical field enhancement and the geometry of the tungsten support.

The collection of these electrons can be avoided by reducing the size of the laser beam, in order to enhance the optical field only at the apex of the sample, or by increasing the ratio between the length of the diamond needle and the thickness of the tungsten tip. Another possibility could be the smoothing of the surface by field evaporation of the atoms from the asperities. By the polarization of a diamond needle at a positive bias of several tens of kilovolts, the atoms from the asperities are field evaporated and the roughness of surface of the needle is strongly improved [30].

Acknowledgments

This work was supported by the French Agence Nationale de la Recherche (ANR), through the program 'Investissements d'Avenir' (ANR-10-LABX-09-01), LabEx EMC3, Efesto project, by the European Union with the European Regional Development Fund (ERDF) and the Regional Council of Normandie. TEM images have been performed using some instruments from GENESIS Plateform. GENESIS is supported by the Région Haute-Normandie, the Métropole Rouen Normandie, the CNRS via LABEX EMC and the French National Research Agency as a part of the program 'Investissements d'avenir' with the reference ANR-11-EQPX-0020. VIK and ANO are grateful for support from Russian Foundation for Basic Research (grant 18-29-19071).

Conflict of interest

There is no conflict to declare.

ORCID iDs

A N Obraztsov https://orcid.org/0000-0001-8017-0496
A Vella https://orcid.org/0000-0003-1501-159X

References

[1] Arbouet A, Caruso G M and Houdellier F 2018 *Advances in Imaging and Electron Physics* vol 207 (Amsterdam: Elsevier) pp 1–72
[2] Ehberger D, Hammer J, Eisele M, Krüger M, Noe J, Högele A and Hommelhoff P 2015 *Phys. Rev. Lett.* 114 227601
[3] Park H S, Baskin J S, Kwon O-H and Zewail A H 2007 *Nano Lett.* 7 2545
[4] Bormann R, Gulde M, Weismann A, Yalunin S and Ropers C 2010 *Phys. Rev. Lett.* 105 147601
[5] Basu A, Swanwick M E, Fomani A A and Velásquez-García L F 2015 *J. Phys. D: Appl. Phys.* 48 225501
[6] Legagneux P, Hudanski L, Ponard P, Bourat C and Schnell J-P 2013 X-rays source comprising at least one electron source combined with a photoelectric control device *US Patent* 8,503,614
[7] Houdellier F, Caruso G M, Weber S, Kociak M and Arbouet A 2018 *Ultramicroscopy* 186 128
[8] Mohammed O F, Yang D-S, Pal S K and Zewail A H 2011 *J. Am. Chem. Soc.* 133 7708
[9] De Heer W A, Chatelain A and Ugarte D 1995 *Science* 270 1179
[10] De Jonge N, Lamy Y, Schoots K and Oosterkamp T H 2002 *Nature* 420 393
[11] Terranova M L, Orlanducci S, Rossi M and Tamburri E 2015 *Nanoscale* 7 5094
[12] Obraztsov A N and Kleshch V I 2009 *J. Nanoelectron. Optoelectron.* 4 207
[13] Houdellier F, Masseboeuf A, Monthioux M and Hÿtch M J 2012 *Carbon* 50 2037
[14] Hudanski L, Minoux E, Gangloff L, Teo K B, Schnell J-P, Xavier S, Robertson J, Milne W I, Pribat D and Legagneux P 2008 *Nanotechnology* 19 105201
[15] Li C *et al* 2017 *Adv. Mater.* 29 1701580
[16] Wang Q, Wang Z, Li J, Huang Y, Li Y, Gu C and Cui Z 2006 *Appl. Phys. Lett.* 89 063105
[17] Hsu C-H and Xu J 2012 *Nanoscale* 4 5293
[18] Porshyn V, Kleshch V, Obraztsova E, Chuvilin A, Lützenkirchen-Hecht D and Obraztsov A 2017 *Appl. Phys. Lett.* 110 182101
[19] Kleshch V I, Purcell S T and Obraztsov A N 2016 *Sci. Rep.* 6 35260
[20] Borz M *et al* 2019 *Nanoscale* 11 6852
[21] Tafel A, Ristein J and Hommelhoff P 2019 *Phys. Rev. Lett.* 123 146802
[22] Obraztsov A N, Kopylov P G, Chuvilin A L and Savenko N V 2009 *Diam. Relat. Mater.* 18 1289
[23] Zolotukhin A, Kopylov P G, Ismagilov R R and Obraztsov A N 2010 *Diam. Relat. Mater.* 19 1007
[24] Torresin O, Borz M, Mauchain J, Blum I, Kleshch V I, Obraztsov A N, Vella A and Chalopin B 2019 *Ultramicroscopy* 202 51–6
[25] Marchand M, Journet C, Adessi C and Purcell S T 2009 *Phys. Rev.* B 80 245425
[26] Lumerical F 2016 *Solutions* (https://support.lumerical.com/hc/en-us/articles/360034914633-FDTD-solver)
[27] Yin Z, Akkerman Z, Yang B and Smith F 1997 *Diam. Relat. Mater.* 6 153
[28] Houard J, Vella A, Vurpillot F and Deconihout B 2010 *Phys. Rev.* B 81 125411
[29] Vella A, Mazumder B, Da Costa G and Deconihout B 2011 *J. Appl. Phys.* 110 044321
[30] Arnoldi L, Spies M, Houard J, Blum I, Etienne A, Ismagilov R, Obraztsov A and Vella A 2018 *Appl. Phys. Lett.* 112 143104